Separation and Purification Technology 249 (2020) 116939

Contents lists available at ScienceDirect

Separation and Purification Technology

journal homepage: www.elsevier.com/locate/seppur

Colloidal fouling in electrodialysis: A neural differential equations model

Bram De Jaegher[a,b,c,d,*], Eneko Larumbe[c], Wim De Schepper[c], Arne Verliefde[b,d], Ingmar Nopens[a,d]

[a] BIOMATH, Department of Data Analysis and Mathematical Modelling, Ghent University, Coupure links 653, 9000 Ghent, Belgium
[b] PaInT, Department of Green Chemistry and Technology, Ghent University, Coupure links 653, 9000 Ghent, Belgium
[c] Flemish Institute for Technological Research (VITO), Boeretang 200, 2400 Mol, Belgium
[d] CAPTURE, Centre for Advanced Process Technology for Urban Resource recovery, Coupure links 653, 9000 Ghent, Belgium

ARTICLE INFO

Keywords:
Electrodialysis
Colloidal fouling
Humic acid
Machine-learning
Neural differential equations

ABSTRACT

The attachment of colloids to the ion-exchange membranes in electrodialysis is an important hurdle when processing bio-based process streams. Previous research showed that fouling strongly depends on the crossflow velocity, the current and the salt concentration of the medium. Predicting the influence of these variables on the fouling rate is challenging due to the complex physics at play and optimising the process conditions to reduce fouling remains a challenge. The objective of this study is the development of a model to predict the dynamic behaviour of electrodialysis fouling under varying process settings to facilitate this optimisation. A neural differential equation is fit to experimental data of an electrodialysis pilot undergoing humic acid fouling. We show that this model can predict the fouling rate even when using a limited set of experimental data. The robustness of the model is demonstrated by a simulation study and a sensitivity analysis indicates that the crossflow velocity is the most important variable influencing the fouling rate (≈ 40%). Both the effect of the current (≈ 20%), the salt concentration (≈ 13%) and their interaction effects are considerable. With the model, the evolution of the stack resistance as a result of membrane fouling can be simulated, facilitating process control or decision-making.

1. Introduction

Decreasing fossil fuel reserves and the environmental consequences related to the exploitation of petroleum products effectuate a shift to a more bio-based and circular economy. The biological feed streams used to produce biochemicals and biofuels are often complex mixtures [1] and the interplay of processes in a circular economy is very intricate. As a consequence, the continuous development of this industry leads to an increasing demand for efficient and selective separation technologies to complement this transition.

As a consequence, electrodialysis (ED) is gaining importance in this field, due to the selective and efficient nature of this process [2]. Furthermore, ED already is a platform for a multitude of derivative processes, e.g. bipolar membrane electrodialysis (EDBM), electrodialysis metathesis, reverse electrodialysis, etc., which gives rise to a lot of applications [2]. The conventional applications of ED are mainly situated in the production of drinking water and the food and drinks industry e.g. demineralisation of milk whey, the removal of tartaric acid in the wine industry, wastewater treatment and seawater desalination [3,4]. There is, however, an increase in both full-scale industrial applications and research interest concerning ED in the (bio-) chemical industry. These new applications range from the detoxification of biomass [5,6] to the selective extraction of amino acids [7] and organic acids from solutions [8,9]. These streams contain organic matter, inorganic matter, colloids, micro-organisms and other macromolecules and the interaction of certain charged and uncharged components with the electric field and the ion-exchange membranes (IEMs) leads to membrane and spacer fouling [10]. Membrane fouling changes the properties of the IEMs and typically process efficiency deteriorates. Given the fact that the cost of cleaning procedures and membrane replacement can account for up to 50% of the operational expenses [11,12], membrane fouling still is an important bottleneck towards the application of ED for the treatment of bio-based process streams [12].

IEM fouling can be defined as “The formation of deposit [sic] on the IEM surface and/or inside the membrane causing an increase in electrical resistance, a decrease in permselectivity and membrane alteration” [12]. Different categories of IEM fouling have been defined; colloidal fouling, organic fouling, membrane poisoning, biofouling and

Abbreviations: ED, electrodialysis; IEM, ion-exchange membrane; SSE, sum of squared errors; MLP, multilayer perceptron

* Corresponding author at: BIOMATH, Department of Data Analysis and Mathematical Modelling, Ghent University, Coupure links 653, 9000 Ghent, Belgium.
E-mail addresses: Bram.DeJaegher@UGent.be (B. De Jaegher), Eneko.Larumbe@Vito.be (E. Larumbe), Wim.DeSchepper@vito.be (W. De Schepper), Arne.Verliefde@UGent.be (A. Verliefde), Ingmar.Nopens@UGent.be (I. Nopens).

https://doi.org/10.1016/j.seppur.2020.116939
Received 14 February 2020; Received in revised form 5 April 2020; Accepted 5 April 2020
Available online 25 May 2020

Nomenclature

α	learning rate ADAM (–)
β_1	hyperparameter ADAM (–)
β_2	hyperparameter ADAM (–)
$\hat{R}$	predicted resistance (Ω)
λ	regularisation parameter (–)
ε_{CV}	cross-validation error (–)
A	parameter (–)
B	parameter (–)
C_e	salt concentration (mol m^{-3})
i	current (A)
K	number of cross-validation folds (–)
M	number of neural netwok parameters (–)
N	number of datapoints in time series (–)
R	stack resistance (Ω)
R_{20}	compensated resistance, 20 °C (Ω)
	ith effect index (–)
S_t	total effect index (–)
T	temperature (°C)
v	crossflow velocity (cm s^{-1})
w	neural network parameters (–)

scaling [12]. Colloidal fouling is the attachment/deposition of non-dissolved suspended solids smaller than 1 μm to/on the IEM. Organic fouling is the adhesion of organic molecules to the membrane surface. These molecules are too large to penetrate the membrane but are still in solution. Membrane poisoning is the penetration of smaller molecules into the IEMs and their adsorption or low mobility leads to a decrease in membrane permselectivity. Biofouling is the growth of micro-organisms on the membrane surface and scaling is the precipitation of inorganic salts. This work focuses on colloidal fouling of the IEMs during ED.

Due to the negatively charged nature of most colloids processed by ED, the fouling intensity of the anion-exchange membrane is the most prominent [2,12]. Colloidal fouling in ED has been subjected to a considerable research effort and is a significant problem for many industrial environmental streams [12]; polyacrylamide fouling was studied by Guo et al. [13] and Sosa-Fernandez et al. [14], the deposition of silica sol was studied by Lee and Moon [15] and a lot of research has been performed for humic acid fouling [16–19]. There are plenty of other colloids in the bio-based and food industry that can lead to IEM fouling [12]. Korngold et al. [17] demonstrated that the rate of colloidal fouling heavily depends on the process settings (crossflow velocity, current density, etc.) and, consequently, good control of these process settings will improve the fouling resilience of ED. A mathematical model capable of predicting the fouling rate as a function of the process settings will facilitate process control and process optimisation.

Even with the clear need for such a model; the number of mechanistic models describing membrane fouling in ED is very limited. Grossman and Sonin [20] developed a generic model to describe the effect of a fouling film on the IEM surface on the limiting current density. Audinos [21] developed a resistance-in-series model for colloidal fouling of ion-selective membranes by grape must and fitted an empiric equation to the resistance increase of the stack. Bdiri et al. [10] relate the membrane conductivity to the conductivity of the fouling layer and solution to better understand the efficacy of cleaning procedures. However, none of the models described above relate the process settings to the fouling rate, defined as electrical resistance or an amount of foulant attached to the membrane, which is essential in predicting ED performance in the presence of foulants. Constructing a fouling model for ED is a challenge due to the abundance and complexity of physical processes at play [2]. This is especially true for humic acid, a model foulant often used in membrane fouling research, which is a complex mixture of organic molecules (both colloid and dissolved) that is difficult to fully characterise [17,22]. As a consequence, a mechanistic description for humic acid fouling in ED is very challenging but when sufficient and good-quality data is available, predictive models using machine learning can perform well at simulating the complex, non-linear interplay of physical phenomena occurring in these fouling processes. Surprisingly, machine learning (neural networks, support vector machine, etc.) has not been applied to model ED or ED fouling, even though its application has been successful to model fouling in a wide range of membrane-based separation processes [23–29]. A model that can predict the fouling rate under varying process conditions will facilitate the development of model-based controllers or decision support tools.

In this paper, we demonstrate the use of neural differential equations to model ED fouling and show that it is a well-suited technique to capture the non-linear phenomena of this dynamic problem. Neural differential equations are an extension of artificial neural networks [30], a popular non-linear machine learning technique that comes in a lot of architectures [31]. To construct a good predictive neural network, it is important to choose the right architecture. In membrane science, multilayer perceptrons (MLPs) are almost exclusively used [24,25,32,33] but when dealing with non-linear dynamic systems this model architecture is not able to deal with the time dependency of the system. When modelling the formation of a fouling layer, the resistance of the membrane in the current timestep is naturally linked to the previous timestep and this information is not easily included when using MLPs. Recurrent neural networks address this issue by including feedback loops in their architecture, allowing time-dependent information to persist [30]. Recurrent neural networks can be expanded in time and it has been shown that these iterative steps are equivalent to the numerical discretisation of a differential equation [34]. Chen et al. [30] elaborated upon this idea and showed that recurrent neural networks can be defined as a differential equation. The advantage is that neural differential equations are a continuous variant of recurrent networks and, as a consequence, can be used on irregularly-sampled data. These neural differential equations have been used as a continuous variant to the existing recurrent and residual neural network applications in image processing [30] but have not yet been used for time series prediction. In this research we present that neural differential equations can be used to simulate the dynamic system of electrodialysis fouling and illustrate the potential of this novel machine learning approach from a chemical engineering perspective.

These neural differential equations are used to model and simulate electrodialysis fouling under varying process conditions. Humic acid is used as a model foulant for colloidal fouling as it is (1) a relevant foulant for bio-based process streams, (2) it is not only relevant for ED but also hampers a lot of other membrane separation processes [35–37] and (3) it is a complex mixture of chemical components both, colloid and dissolved, [22] that complicates the construction of a mechanistic model and emphasizes the power of these black-box differential equations. Humic acid fouling experiments were performed on a pilot ED installation to train and validate this model. For this, the evolution of the electrical resistance of the pilot ED stack was monitored when the salt concentration of the medium, the crossflow velocity and the current is varied. The potential of neural differential equations is critically analysed concerning interpolation and extrapolation in the time domain and for the input variables. The model is subsequently used for system analysis to provide insight into the effect of the process settings on the fouling behaviour. For this, the fouling rate, defined as the change in stack resistance, is mapped as a function of the process variables to identify the settings that lead to fast and slow fouling. Furthermore, a sensitivity analysis is performed to determine the most influential process variables and characterise the non-linearity of and the interaction effects between the process variables. This sensitivity

analysis provides insight into which process setting to focus on to improve the fouling resilience of the ED.

2. Materials and methods

2.1. Setup

The experimental tests are performed using an automated ED pilot installation (VITO, Belgium). The pilot consists of three circulation loops separating the concentrate, diluate and electrode rinsing solutions. The diluate and concentrate compartments are connected to the same storage tank (≈25L) to ensure a constant salt concentration. The electrolyte rinsing circuit is fed by a separate tank (≈25L). The concentrate, diluate and electrolyte rinsing circuit are driven by three separate pumps (GM-V IWAKI, USA - PID controlled). The concentrate and diluate circuits have to be fed by a separate pump to ensure an equal flow rate regardless of the fouling severity in the stack. A 0.1 M solution of Na_2SO_4 is used as electrode rinsing solution and is fed by the third pump to the anode and cathode compartments, in series. In the pilot, the temperature, pH, flow rate, conductivity are measured before and after the ED stack for all circuits. The pressure, tank volumes, current and voltage are also monitored. The data acquisition and control is handled by Mefias, a LabVIEW-based control software (VITO, Belgium). An FT-ED(R)-100–4 (ED100, FuMA-Tech, Germany) ED stack is built with three cell pairs of alternating cation- and anion-exchange membranes, starting and ending with a cation-exchange membrane. The cation- and anion-exchange membranes used in this study are homogeneous PCA-SK and PCA-SA membranes (PCA GmBh, Germany), respectively, both with a surface area of 100 cm^2. The ED stack is powered by a power supply operated as a galvanostat (SM 3000 - Delta electronika, the Netherlands). Humic acid sodium salt (Sigma–Aldrich, USA) is used as the fouling component and a concentration of 1 g/L is maintained for all experiments.

2.2. Methodology

The goal of this study is the development of a model to capture and predict the dynamic behaviour of electrodialysis fouling under varying process settings. The three process variables that are input variables to the model are the salt concentration (C_e, M) in the foulant solution, the crossflow velocity (v, cm/s) in the stack and the applied current density (i, A). These were varied while monitoring the resistance of the stack as a measure for the fouling severity. The experiments were designed as a 3-factor full-factorial with 5 levels for the current density, 4 levels for the crossflow velocity and 3 levels for the concentration of salt and, as such, 60 experiments (time series) were carried out. However, at some process settings the severe fouling rate lead to short timeseries not suitable to be used in the data processing and modelling strategy discussed in what follows. These experiments were dropped, retaining a total of 22 experiments, according to the experimental design depicted in Fig. 1. Each of the points in the experimental design (Fig. 1) represents a time series of the stack resistance during the fouling experiment for a fixed set of crossflow velocity, current density and salt concentration. It should be noted that the design of experiment requirements for machine learning are less stringent than experimental design methodologies that focus on the statistical inference of treatment parameters. The main goal is to construct a predictive model given a dataset that covers a sufficiently large input space of the underlying system. The design of experiments presented in Fig. 1 provides an adequate range of input variables to train the model which is discussed in Section 3.

The data acquisition was performed at a sampling interval of 15 s. Some of the experimental conditions presented in Fig. 1 lead to a high fouling rate and those experiments were terminated early as the maximum potential of the power supply was reached. So the length of the experiments varies from a few minutes to a maximum of 1.5 h (360 data points). All fouling experiments are performed for 1.5 h after which the polarity of the electrodes is inverted for 1.5 h to clean the membranes and bring the system back to its original state. To ensure the reversibility of the fouling layer, a current sweep is performed periodically to compare the limiting current density and membrane resistance of the virgin system. The membranes are replaced with new membranes when the salt concentration of the medium is changed.

As temperature fluctuations due to heat generation from ohmic dissipation and environmental factors have a considerable effect on the electrical conductivity of electrolyte solutions a non-linear temperature compensation is performed. This compensation takes into account the effect of temperature on water viscosity and ion diffusivity [38],

$$R_{20} = 0.889 \cdot 10^{A/B} R \quad (1)$$

with R_{20} the compensated resistance at 20 °C, R the measured resistance. A and B are temperature-dependent parameters and are

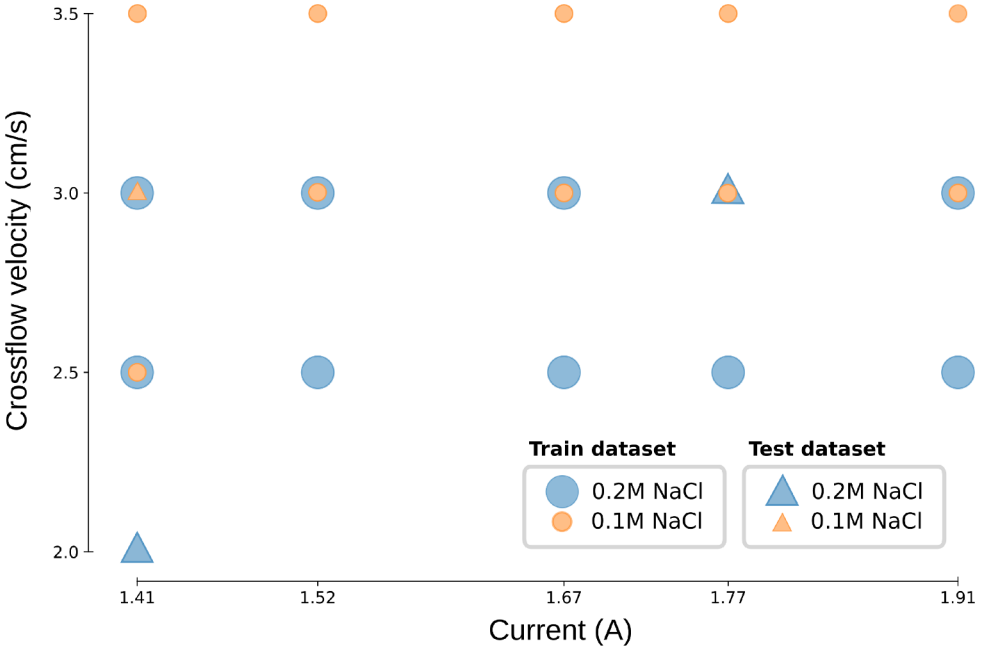

Fig. 1. Experimental design of the 22 experiments performed in this study. Each point represents an experiment and the three degrees of freedom are the crossflow velocity (*y*-axis), the current density applied (*x*-axis) and the concentration of NaCl added to the fouling solution (size and colour of the markers). Experiments that are omitted from the training dataset and used for model testing are denoted by triangular markers.

computed as follows [38],

$$A = 1.37(T - 20) + 8.36{\cdot}10^{-4}(T - 20)^2 \quad (2)$$

$$B = 109 + T \quad (3)$$

with T the temperature (°C). By applying this compensation, the effect of temperature fluctuations is eliminated.

To reduce the sensor noise the data was processed with a simple moving-average filter with a window size of 10 data points. All time series must consist of an equal number of data points to ensure an equal contribution to the loss function (Eq. (5)). Accordingly, all time series were resampled to 20 data points over the total length of the experiment.

To ensure that the ED installation is being operated well within the underlimiting current region, a series of experiments was performed, prior to the experimental design, to determine the limiting current density at the lowest concentration of salt and the lowest crossflow velocity. A safety margin of 20% is used which fixes the maximum current used in this study to 1.91A. All experimental conditions presented in Fig. 1 lie withing this safety margin as the limiting current increases with the electrolyte strength and crossflow velocity. The experimental conditions are chosen to resemble values applied in the nominal operation of ED. A concentration of humic acid (1 g/L) results in severe fouling conditions which are ideal for these accelerated fouling tests. The current range tested here (1.41A-1.91A) is quite narrow but in Section 3.1, we show that this region is wide enough to demonstrate two very distinct fouling behaviours.

To summarise the experimental procedure, 22 time series of the stack resistance were obtained while varying the crossflow velocity, current and salt concentration. Membranes are cleaned in between experiments by reversing the polarity of the electrodes. The acquired time series are compensated with respect to temperature variation, processed by a moving-average filter and resampled to 20 time points over the entire timespan of each experiment.

2.3. Neural differential equations

The neural differential equation presented in this paper follows the definition of Chen et al. [30], an ordinary differential equation with an artificial neural network on the right-hand side of the equation. We will touch on the key building blocks to describe our system but an in-depth mathematical description of neural networks is out of scope.

The resistance over the electrodialysis stack, $\mathbf{R}(t)$ (Ω), is the output variable of the model. During ED, humic acid forms a fouling layer on the IEMs, reducing the diffusivity and thus the conductivity in the channels [39]. This phenomenon can easily be measured as the increase in stack resistance and after the removing the effects of the temperature (Eq. (1)) it is a good indicator for the amount of humic acid attached to the ion-exchange membranes. Korngold et al. [17] showed that the fouling rate (change in membrane resistance) is heavily influenced by the crossflow velocity (v), the current (i) and the concentration of NaCl in the fouling solution (C_e) which are defined as input variables to the model. A neural differential equation is constructed that models the change in stack resistance $\left(\frac{d\mathbf{R}(t)}{dt},\ \Omega/\mathrm{h}\right)$ as a function of v, i and C_e and $\mathbf{R}(t)$,

$$\frac{d\mathbf{R}(t)}{dt} = f(\mathbf{R}(t),\ v,\ i,\ C_e), \quad (4)$$

where f represents a feed-forward neural network, $\mathbf{R}(t)$ is in the right hand side of the equation because the fouling rate $\left(\frac{d\mathbf{R}(t)}{dt}\right)$ at a certain time is influenced by the fouling state at that time ($\mathbf{R}(t)$).

The neural network (Eq. (4), RHS) consists of four inputs, one fully-connected, four neuron, hidden layer along with two fully-connected, eight neuron, hidden layers and an output layer. Sigmoid activation functions are used for each layer but the last. In the age of deep learning, this is considered a tiny neural network but the results show that a small-sized neural differential equation can still yield an adequate model structure to accurately capture the dynamic and non-linear behaviour of electrodialysis fouling. Even with the presence of a neural network, Eq. (4) still is an ordinary differential equation and is solved in time to obtain ($\mathbf{R}(t)$), using the explicit Runge–Kutta 3(2) solver [40] that allows for an adaptive step size. To further clarify the mathematical structure of and solution procedure for Eq. (4), a schematic overview of this neural differential equation and the coupling with ODE-solver is depicted in Fig. 2. This procedure is implemented in the Julia programming language [41] where an interface between the neural network and the differential equations solver suite is provided by the *DiffEqFlux.jl* package [42].

The neural differential equation (Eq. (4)) is fit to the training data by iteratively changing the parameters of the neural network while solving the differential equation over time. Each iteration, the predicted time series is compared to the measurements by using the sum of squared errors (SSE) and an L1-regularisation term is added to avoid overfitting. This term penalises the parameters in the neural network and limits the model complexity. Finally, the following loss function is

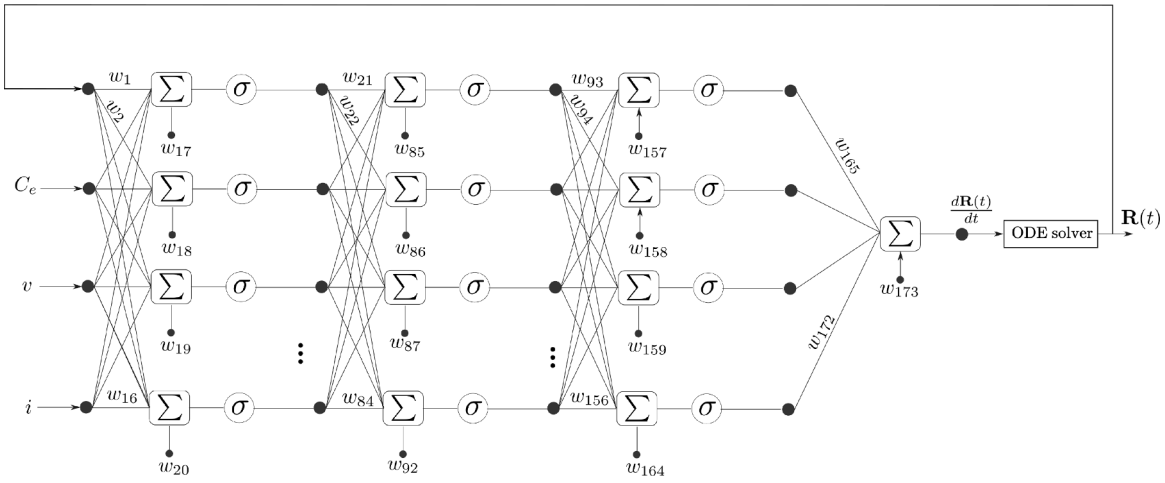

Fig. 2. Detailed diagram of the neural differential equation. Summations are denoted by $\sum$, the sigmoid activation function by σ and the parameters of the network by w_k. The input variables of the neural differential equation are the stack resistance at the current time $\mathbf{R}(t)$, the salt concentration (C_e) the crossflow velocity (v) and the current density (i). The neural network outputs a time derivative, the change of stack resistance in time, which is fed to a differential equation solver and the neural differential equation is solved over time.

obtained,

$$L = \sum_{j=1}^{N} (\mathbf{R}_j - \hat{\mathbf{R}}_j)^2 + \lambda \sum_{k=1}^{M} |w_k|, \tag{5}$$

with $\mathbf{R}(t)$ the experimental stack resistance, $\hat{\mathbf{R}}(t)$ the predicted stack resistance, λ the regularisation parameter, w the parameters of the neural network, N the number of datapoints spanning all timeseries and M the number of parameters (w_k) in the neural network ($M = 173$).

The loss function (Eq. (5)) is minimised with a gradient-based stochastic ADAM optimiser with a learning rate (α) of 0.03 and default hyperparameters values ($\beta_1 = 0.9$, $\beta_2 = 0.999$) [43]. In the loss function, λ, balances the model complexity and the training error. A high value of this hyperparameter reduces the complexity of the neural network by bringing the parameter values down to zero which leads to underfitting. For high values of λ, the penalty on model complexity is less stringent and the neural network tends to overfit on the training data. This is called the bias-variance tradeoff and by tuning the value of λ, a model is obtained that generalises well to new data. In the experimental design (Fig. 1), it was indicated that the experimental data is split into a training and test set but to evaluate the optimal value of λ a third dataset is required. To avoid a further partitioning of the training set into a training and validation set, leave-one-out cross-validation is performed along with a two-step grid-search. Six values of λ were tested and for each value, the cross-validation error (Eq. (6)) is computed by sequentially training the model while leaving out another time series from the training set (fold). The cross-validation error estimate is computed by summing the SSE for each fold according to Eq. (6). A schematic representation of leave-one-out cross-validation is depicted in Fig. 3.

$$\varepsilon_{CV} = \frac{1}{K} \sum_{l=1}^{K} (\mathbf{R}_l - \hat{\mathbf{R}}_l)^2 \tag{6}$$

where ε_{CV} is the cross-validation error, K is the number of folds and $\hat{\mathbf{R}}_l$ and $\mathbf{R}_l$ the withheld data and model prediction of the withheld data for the l-th fold, respectively.

2.4. Sensitivity analysis

The influence of each of the input variables (Ce, v, i) on the fouling rate, defined as the increase in stack resistance after 0.5 h, is investigated using a Sobol sensitivity analysis. Sobol's methodology yields a set of indices that attribute the variance of the output variable (resistance change after 0.5 h) to linear, non-linear and interaction effects of the input variables. It provides a quantitative estimation of the relative importance of each of the factors and separates linear effects from non-linear and interaction effects [44,45]. So next to identifying the most influential input variables, it provides information on the non-linearity which can justify the choice of neural differential equations over a much simpler autoregressive integrated moving average models or multivariate linear regression model. The mathematics of Sobol's method are elaborated upon in Appendix A. Sobol's method is a variance-based methodology and a sufficiently large number of simulations is required to accurately estimate the Sobol indices. For each of the Sobol indices, an N of 200.000 is chosen which results in a total of 1.000.000 simulations to estimate each Sobol index. The fouling rate is the output variable for the sensitivity analysis and is represented here by the resistance increase after 0.5 h. From this, the first order ($S_{1,i}$), second-order ($S_{2,i}$) and total Sobol indices ($S_{T,i}$) are computed.

3. Results & discussion

3.1. Experiments

The experiments were performed according to the experimental design depicted in Fig. 1 which consists of 22 experimental time series, three of which were withheld as a test dataset to evaluate the model's performance. A subset of the experimental time series is depicted in Fig. 4 where the effect of the different input variables has been separated. A full description of the experimental data is elaborated upon by De Jaegher et al. [46].

The effect of the current on the fouling rate is presented in Fig. 4(a), the fouling rate increases with the current density but the relation is not linear. These results agree with Korngold et al. [17] where three current densities were tested and non-linear behaviour of the fouling rate as a function of the current density was reported. The results of Korngold et al. [17] were obtained with a different stack design, a different type of humic acid (out-of-production) and different IEMs, so a side-by-side comparison is not possible. It can also be seen that at low currents (1.4A-1.7A), the fouling only slightly increases with an increase in current. At higher currents, the effect of the current is more pronounced. This is expectedly caused by the formation of a membrane sandwich of the negatively-charged fouling layer with the positively-charged anion-exchange membrane [39]. This bipolar membrane structure is known to promote water splitting, where the diluate side receives the H^+ ions leading to a decrease in pH. The solubility of humic acid decreases with the pH so water splitting promotes humic acid fouling on the AEMs [17,39]. This auto-catalytic effect is believed to drive the exponential increase in fouling resistance as a decrease in pH was noticed in the diluate compartment [46]. For a current of 1.91A, the time series are too short and the fouling too severe to make any conclusions on the occurrence of an autocatalytic fouling phase. Saturation of the fouling rate may occur due to an interaction of the fouling layer with the fluid phase (shear stresses). Decreasing the crossflow velocity leads to increasing fouling rates and also here the autocatalytic effect can be noticed by the strong non-linear increase of the stack resistance (Fig. 4(b)). There is also an effect of the salt concentration on the fouling rate (Fig. 4(c)), where a low salt concentration leads to a high fouling rate, in agreement with Korngold et al. [17] where three salt concentrations were tested.

Finally, the experimental design enables the exploration of interaction effects between the different input variables as discussed in Section 3.2 and a quantitative analysis of the influence of the input variables on the fouling rate is elaborated on in the sensitivity analysis (Section 3.3). From these results, it can be seen that the occurrence of an exponential fouling phase leads to a sudden and fast increase of the stack resistance. Hence, it is important to tune the process conditions to hold off the exponential phase to prolong the active cycles of the ED. The balance between slow and fast fouling is fragile, which is made evident by the narrow range of tested current densities.

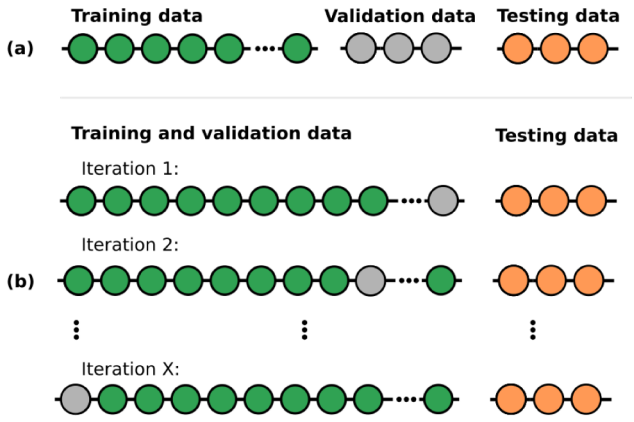

Fig. 3. The subdivision of the data according to the leave-one-out cross-validation strategy followed (b) compared to a three-way split of the dataset in a training, validation and test set (a).

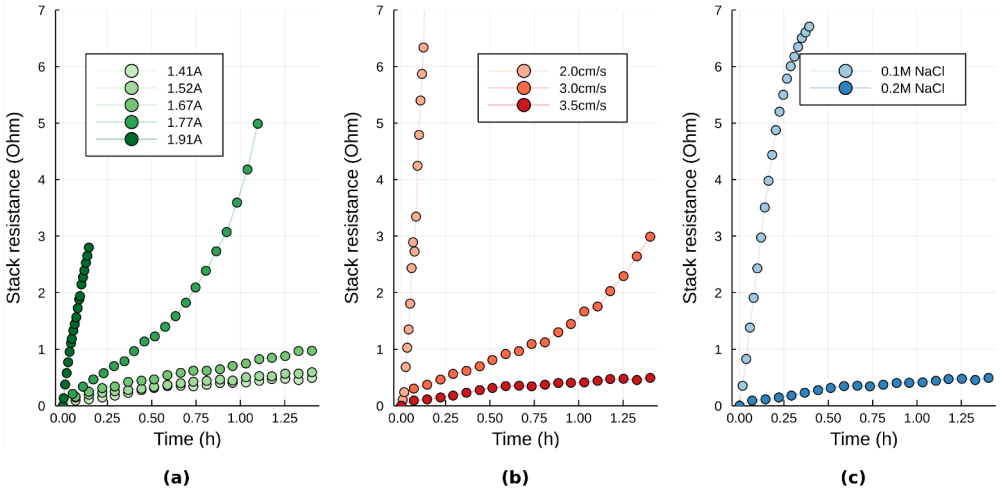

Fig. 4. The stack resistance as a function of time for a salt concentration of 0.2 M, crossflow velocity of 3.0 cm/s and a varying current (left), a salt concentration of 0.2 M, current of 1.41A and a varying crossflow velocity (middle) and a crossflow velocity of 3.0 cm/s a current of 1.41A and a varying salt concentration (right).

3.2. Model training, cross-validation and testing

The training predictions are displayed to illustrate the behaviour of the model over a range of input values and demonstrate the behaviour of the model when varying the input variables. It is important to note that conclusions on the model accuracy are solely based on predictions of the test data.

Six values of the regularisation parameter, λ, were tested using leave-one-out cross-validation. The cross-validation error was estimated using a two-step grid-search where the SSE is averaged over the folds (Eq. (6)). The results of the cross-validation are presented in Table 1. It can be seen that a λ of 5e-6 leads to the lowest cross-validation error and this λ-value is selected as the optimal value. This error estimate can be interpreted as the generalisation error and the model trained with this λ should lead to the best balance between under- and overfitting. Hence, the results presented in the remainder of this study are obtained with the model trained with the optimal λ-value.

The goodness-of-fit, defined by the SSE, with respect to both training data and test data for each time series are summarised in Appendix B. The predictions of the stack resistance in time at a constant salt concentration of 0.2 M NaCl and crossflow velocity of 3.0 cm/s for a varying current density are depicted in Fig. 5. The time series at 1.77A is part of the test dataset and is chosen as it lies in the middle of the experimental design. Fig. 5 shows that the model is able to accurately predict the test data. The non-linear effect of the current density is captured in the dynamics but also the auto-catalytic effect that starts at 0.5 h is predicted. The distinct curvature of the test series cannot be found in the other time series in Fig. 5 but the model learned this behaviour from the other time series (e.g. Fig. 6, 2.5 cm/s). Not unexpectedly, the training data is almost perfectly predicted.

The predictions for a changing crossflow velocity, at a constant current density of 1.41A and salt concentration of 0.2 M, is depicted in Fig. 6. The fouling rate of the test series at 2.0 cm/s is overestimated but considering that this experiment is situated in a corner of the experimental design, this is a satisfying result. The evolution of the fouling rate at 2.5 cm/s is interesting as it again illustrates the autocatalytic nature of this process.

Fig. 7 shows the predictions of the stack resistance at a constant salt concentration of 0.1 M NaCl and crossflow velocity of 3.0 cm/s for a varying current density. For this set, the model performance is considerably worse as the fouling rate is overestimated and the curvature of the prediction is wrong. The model predicts the occurrence of the autocatalytic effect while it is not present under the current experimental conditions. At this salt concentration, the fouling was very severe for all current densities which resulted in a short time series with significantly less information on the curvature and the occurrence of an exponential phase, compared to the data of 2 M NaCl. Running the experiments for a longer period could alleviate this issue but the limitations of the power supply were reached. Nevertheless, in Section 3.3 we show that a slight decrease in current leads to a better prediction and that 1.41A lays close to the value at which the switch to an exponential fouling regime occurs. It is not an artefact as it is also visible for low current densities at 0.2 M NaCl (Fig. 5). This curvature at low currents can also be seen in the experiments of Korngold et al. [17]. Although never described for ED, the occurrence of an operational regime at which the fouling stagnates is valuable. In membrane filtration, the concept of critical flux is well-known, i.e. a transmembrane flux below which there is no decline in transmembrane pressure. The value of the critical flux depends on the hydrodynamic conditions and likely other variables [47]. For ED this could be defined as a critical current density below which no increase in membrane resistance is noticeable. At the critical current density, the fouling deposition is counteracted by the shear stresses but further experimentation with long-term fouling tests at low fouling rates is required to confirm the occurrence of a critical current density for ED.

In Fig. 7 the stabilisation of the stack resistance is not predicted by the model. This can be explained by the fact that only a few of the experimental conditions exhibit this downward trend, mostly at low current densities. For most of the experiments the effect is subtle (Fig. 5, 1.41–1.66A) and the model can adequately describe this by a monotonic increasing response (Fig. 11). Increasing the model complexity, by lowering the λ or adding more layers and neurons, should improve these of the fouling layer stabilisation but would require more

Table 1
The cross-validation error of the model (SSE) obtained via leave-one-out cross-validation for different values of λ. $\lambda = 5e-6$ leads to the lowest cross-validation error.

λ	ε_{CV}
10^{-7}	1.09
10^{-6}	0.62
$5{\cdot}10^{-6}$	**0.42**
10^{-5}	1.54
10^{-4}	2.47
10^{-3}	4.14

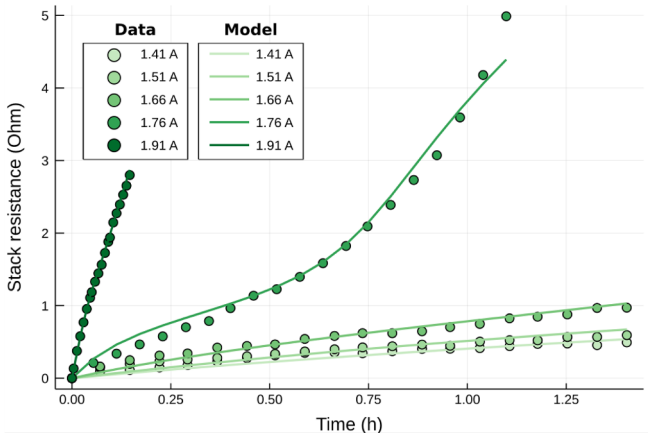

Fig. 5. Prediction of the stack resistance in time at a salt concentration of 0.2 M NaCl and a crossflow velocity of 3.0 cm/s. The current density was varied as indicated by the legend. The model prediction at 1.76A is the test dataset, all other predictions are from the training set. The data is depicted with circular markers and the model predictions as a full line.

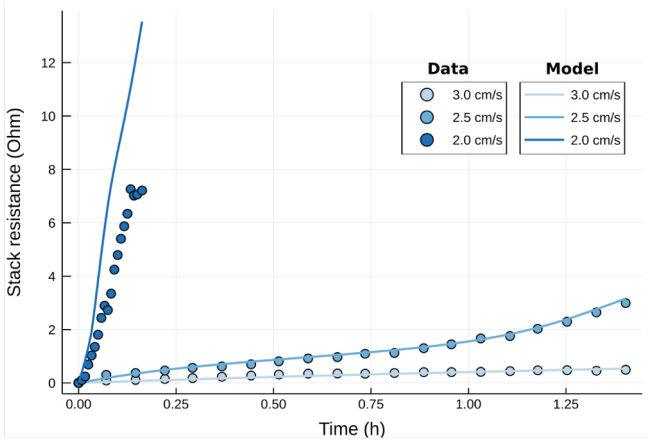

Fig. 6. Prediction of the stack resistance in time at a salt concentration of 0.2 M NaCl and a current density of 1.41A. The crossflow velocity was varied as indicated by the legend. The model prediction at 2.0 cm/s is part of the test dataset, all other predictions are from the training set. The data is depicted with circular markers and the model predictions as a full line.

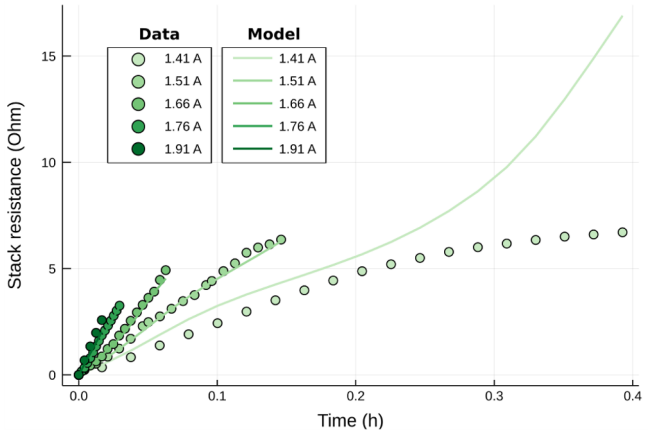

Fig. 7. Prediction of the stack resistance in time at a salt concentration of 0.1 M NaCl and a crossflow velocity of 3.0 cm/s. The current density was varied as indicated by the legend. The model prediction at 1.41A is the test dataset, all other predictions are from the training set. The data is depicted with circular markers and the model predictions as a full line.

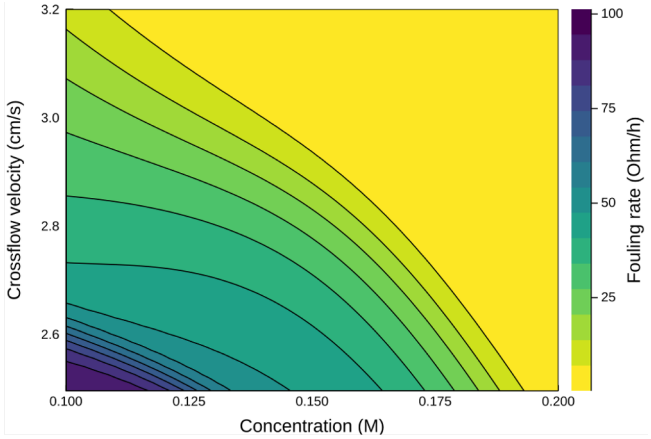

Fig. 8. The initial fouling rate of the stack as a function of the crossflow velocity (y-axis) and the salt concentration (x-axis). For a constant current density of 1.41A.

experiments to train the model. Additionally, the stabilisation of the fouling layer is a long-term effect that is likely to occur at low fouling rates due to the formation of a loose fouling layer and is not sufficiently captured by the short-term data from these accelerated fouling tests.

The simulations presented above (Figs. 5–7), were obtained by solving the neural differential equation (Eq. (4)) for time. However, without solving, Eq. (4) provides a continuous description of the initial fouling rate ($\frac{d\mathbf{R}(t)}{dt}|^{t=0}$) as a function of crossflow velocity, current and salt concentration. Next to the initial fouling rate, these contours can also be computed for the increase in resistance after a certain period. This gives a different insight into fouling behaviour, depending on what information is sought, e.g. the long-term fouling prediction. Fig. 8 shows the initial fouling rate of the stack as a function of the crossflow velocity and the salt concentration. Low crossflow velocities and low concentration lead to a high fouling rate. The interaction effect of both input variables is also clear as a purely linear system without interaction between the input variables would lead to equidistant contours. The effect of the current and crossflow velocity are depicted in Fig. 9, low current densities lead to a low fouling rate and also there is an interaction effect between the current and crossflow velocity. Lastly, the effect of the current and salt concentration are depicted in Fig. 10. The contribution of both variables has already been discussed but also here a strong interaction effect is apparent. Quantification of the linear, non-linear and interaction effects is further elaborated on in Section 3.3. Low salt concentrations, low crossflow velocities and high current densities drive concentration polarisation. Since we show that these

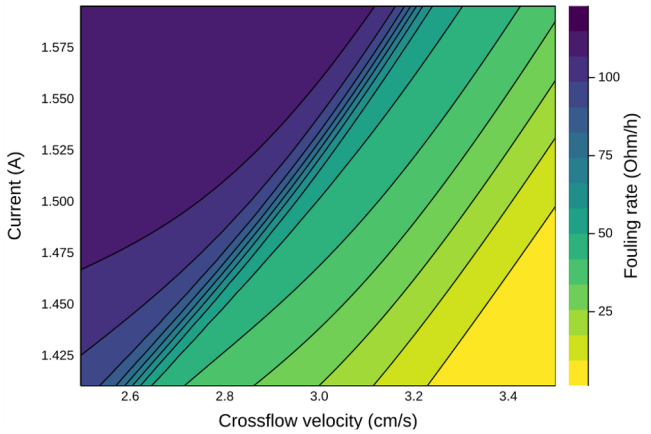

Fig. 9. The initial fouling rate of the stack as a function of the current (y-axis) and the crossflow velocity (x-axis). For a constant salt concentration of 0.1 M.

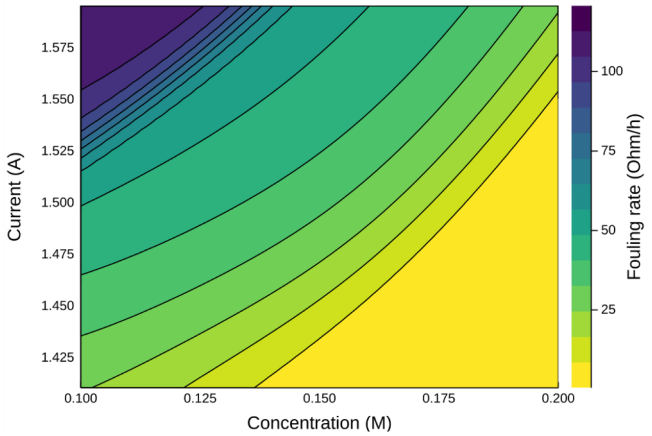

Fig. 10. The initial fouling rate of the stack as a function of the current (y-axis) and the salt concentration (x-axis). For a constant crossflow velocity of 3 cm/s.

conditions relate to high fouling rates it seems that the fouling rate is correlated to concentration polarisation and, as an extension, the limiting current density which is also heavily influenced by these variables [48].

It can be concluded that high crossflow velocities, low current densities and high salt concentrations lead to a reduced fouling rate. There are, however, a few important notes. The salt concentration can often not be chosen freely, as it follows from the characteristics of the stream to be treated. High crossflow velocities lead to high operational expenses due to pumping costs and a low current leads to slow desalination. Taking into account these constraints, it is clear to see that a decision on the optimal conditions for ED is not straightforward. This illustrates the need for a good model as a decision-support system. We provide such a model but a good quantification of all expenses at play is needed to determine the process conditions for the operation of an ED installation and should be the focus for future research.

The lack of predictive power when the inputs are outside the range of the training dataset is often regarded as the major disadvantage of machine learning algorithms [49]. To illustrate the robustness of the applied methodology, additional simulations were performed to demonstrate the system dynamics during interpolation and extrapolation of the input variables (C_e, v, i) and while extrapolating in time. The behaviour of the model when extrapolating in time was investigated by solving Eq. (4) beyond the maximum experimental duration of 1.5 h. The results are depicted in Fig. 11(a). The extrapolation in time is smooth with no abrupt changes of the resistance. At 1.41A and 1.52A the exponential regime is not present and a stable fouling regime is predicted by the model. Fig. 11(b) illustrates the behaviour of extrapolation with respect to the current. Additional simulations were performed at 1.34A, 1.37A and 1.41A which fall outside the trained domain (1.41–1.91A) and the simulations were solved for a time duration of 0.4 h. The experiment at 1.41A is part of the test set and was not used for the training of the model. In Section 3.2 it was discussed that the model overpredicts the resistance change and a transition to the exponential fouling regime was predicted which does not occur in the data. For the former, it is clear that the model (and the ED pilot) is very sensitive to the value of current. When the current is decreased from 1.41A to 1.40A, a deviation of 0.7%, the prediction improves considerably. The start of the exponential fouling regime is still a discrepancy and is likely the effect of data scarcity due to the limitations of the power supply. Nevertheless, it is clear that for extrapolation of the input variables and time, there are no discontinuities or abrupt changes in the predicted time series which is a desirable property for a robust model. It is concluded that for modelling and simulation of colloidal fouling during ED this methodology can extrapolate smoothly in time. The model captures the trends well for most of the test cases. However, the length of the experiments is an important factor to take into account when training these neural differential equations. If one looks to model long-term fouling behaviour this should also be reflected in the experiments.

3.3. Input sensitivity analysis (Sobol)

Since the model fits well to the training and test data and the model robustness was demonstrated, this model is considered a good approximator of the system and can be used for system analysis. To investigate the influence of each of the input variables (C_e, v, i) on the fouling rate, a Sobol sensitivity analysis was performed. Sobol's method yields a set of indices that attribute the variance of the output variable (resistance change after 0.5 h) to linear, non-linear and interaction effects and is summarised in Table 2. The first-order effects (S_1) yield information on the direct, linear contribution of each input variable. The crossflow velocity (v) has the highest linear effect on the fouling rate followed by the current (i) and salt concentration (C_e). The sum of these indices should be smaller than or equal to unity. This upper limit is achieved when the model is purely additive. In the case presented here 73% of the output variance can be attributed to linear effects with a contribution of 41%, 19% and 13% for, respectively, the crossflow velocity, the current and the salt concentration. A conclusion on the overall importance of the input variables can be found in the total effect indices (S_t) which summarises the total contribution of each input variable, including all non-linear and interaction effects. It is important to note that the sum of S_t is larger than one because interaction effects between variables are attributed more than once. With a total effect index of 0.68 for the crossflow velocity compared to 0.36 for the salt

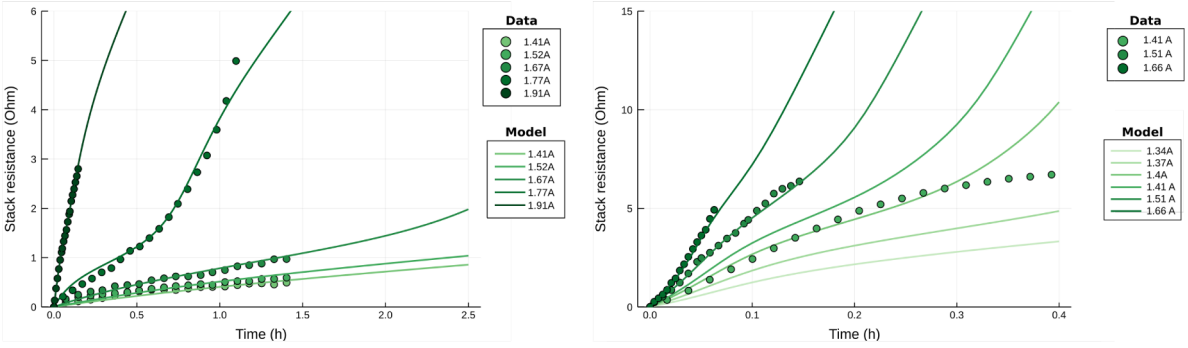

Fig. 11. Prediction of the stack resistance in time at a salt concentration of 0.2 M NaCl and a crossflow velocity of 3.0 cm/s (a) and a salt concentration of 0.1 M NaCl and a crossflow velocity of 3.0 cm/s (b). The experimental data are denoted by circular markers and the model predictions are displayed with a full line. The current density was varied as indicated by the legend.

Table 2
The Sobol indices computed ($N = 200.000$) for each of the input variables (i, v, C_e). The first-order effects (S_1) yield information of the linear contribution each input variable, separately. The second-order effects (S_2) lumps the second-order non-linear effects and second-order interaction effects. The total effect index (S_t) yields the total contribution of each input variable including all non-linear and interaction effects. The output variance is determined based on the stack resistance change after 0.5 h.

Variable	S_1	S_2	S_t	$S_t - S_1$
i	0.186	0.032	0.326	0.140
v	0.413	0.002	0.680	0.267
C_e	0.131	0.127	0.360	0.230
Sum	0.730	0.161	1.368	0.637

concentration and 0.326 for the current density, it can be seen that the crossflow velocity is the most important variable to optimise to reduce fouling within the range of tested process settings. The effect of the current and the salt concentration still is considerable and should not be ignored. Finally, all non-linear and interaction effects are quantified by subtracting the linear effects from the total effects ($S_t - S_1$). It is clear that there are considerable non-linear effects and interaction effects for all input variables. This justifies the use of a non-linear model such as a neural network to model electrodialysis fouling. Moreover, the performance of such a simple model was also investigated. For this a least-squares multiple linear regression was performed with first-order interaction effects included Eq. (7). The results are summarised in Table 3. It can be seen that the performance is considerably worse on both training and test data, multiple linear regression is not able to capture the non-linear and interaction effects in the input variables.

4. Conclusions

This study demonstrates the use of neural differential equations, a novel machine learning methodology to model the effect of humic acid fouling during ED. A total of 22 experiments were performed where the crossflow velocity, current and salt concentration on the fouling was varied while monitoring the stack resistance to train and validate the model. We show that the model can capture the dynamics of the problem and make accurate predictions on withheld data. The properties of this model were analysed critically by performing additional simulations when extrapolating for both the time and the current. As it is a data-driven approach, the main disadvantage of the model is that to achieve prective power you need good-quality data over a sufficiently long time period and a sufficiently large input range. However, we show that neural differential equations extrapolate well to new inputs and no discontinuities or abrupt changes occurred which demonstrate that neural differential equations are a well-suited and robust methodology to simulate colloidal fouling in ED. A system analysis was executed where the effect of the input variables on the fouling behaviour is quantified. Using a Sobol sensitivity analysis, the direct, linear effect of the crossflow velocity is quantified as 41% compared to 18.6% and 13.1% for the current and the salt concentration respectively. The interaction and non-linear effects follow the same trend but are less pronounced. Nonetheless, all three variables have a considerable effect on the fouling behaviour which is confirmed by previous research. It can be concluded that to reduce the fouling rate, the crossflow velocity is the most important variable to optimise within the range of tested process settings. From both the experiments and the model, it is clear that high crossflow velocities, low current densities and high salt concentrations lead to a reduced fouling rate.

CRediT authorship contribution statement

Bram De Jaegher: Conceptualization, Methodology, Software, Visualization, Writing - original draft. **Eneko Larumbe:** Investigation. **Wim De Schepper:** Writing - review & editing, Supervision, Resources, Funding acquisition. **Arne Verliefde:** Writing - review & editing, Resources. **Ingmar Nopens:** Writing - review & editing, Supervision, Project administration.

Declaration of Competing Interest

The authors declare that they have no known competing financial

Table 3
Summary of the experiments and process settings used, salt concentration in M (Salt conc.), current in A (Current), crossflow velocity in cm/s (Velo.). For each experiment, it is indicated whether it was used for training, cross-validation or testing. The SSE between prediction and data is given for each of the time series for both the neural ODE (NN) and least-squares multiple regression (LR).

Experiment	Salt conc.	Current	Velo.	Dataset	SSE (NN)	SSE (LR)
1	0.2	1.41	3.0	Train + CV	0.002	8513.971
2	0.2	1.52	3.0	Train + CV	0.004	1525.245
3	0.2	1.67	3.0	Train + CV	0.003	1132.671
4	0.2	1.77	3.0	Test	0.030	3904.029
5	0.2	1.91	3.0	Train + CV	0.001	85.829
6	0.2	1.41	2.5	Train + CV	0.006	3167.398
7	0.2	1.52	2.5	Train + CV	0.008	315.447
8	0.2	1.67	2.5	Train + CV	0.013	0.038
9	0.2	1.77	2.5	Train + CV	0.043	0.576
10	0.2	1.91	2.5	Train + CV	0.181	0.264
11	0.2	1.41	2.0	Test	11.884	60.328
12	0.1	1.41	3.0	Test	0.022	2.666
13	0.1	1.51	3.0	Train + CV	13.466	244.548
14	0.1	1.66	3.0	Train + CV	0.029	5.003
15	0.1	1.76	3.0	Train + CV	0.024	0.558
16	0.1	1.91	3.0	Train + CV	0.007	0.914
17	0.1	1.41	2.5	Train + CV	0.128	0.699
18	0.1	1.41	3.5	Train + CV	0.106	271.903
19	0.1	1.53	3.5	Train + CV	0.004	2121.917
20	0.1	1.67	3.5	Train + CV	0.133	4.736
21	0.1	1.77	3.5	Train + CV	0.013	239.302
22	0.1	1.91	3.5	Train + CV	0.008	12.407

interests or personal relationships that could have appeared to influence the work reported in this paper.

Acknowledgment

Funding: This work was supported by the Flemish institute for technological research (VITO).

The authors would further like to acknowledge prof. Francis wyffels of the Faculty of Engineering and Architecture, Department of Electronics and Information Systems for providing input to this work and proofreading this article.

Appendix A

A.1. The Sobol method for global sensitivity analysis

The Sobol method is a variance-based sensitivity analysis which decomposes the variance of the output of the model into fractions which can be attributed to inputs or sets of inputs. This method allows to estimate the individual parameter's sensitivities (first order indices) but also quantifies the sensitivity from the interaction between the parameters and the non-linearity of the parameters [44,45]. A non-linear model is assumed that can be decomposed as follows [45],

$$Y = f_0 + \sum_{i=1}^{d} f_i(X_i) + \sum_{i<j}^{d} f_{ij}(X_i, X_j)...+f_{1,2...d}(X_1, X_2, ..X_d),$$

with Y the ouput of the model, f_0 a constant, f_i is a function of X_i, f_{ij} a function of X_i and X_j, etc. The variance of Y ($Var(Y)$) can be decomposed as,

$$Var(Y) = \sum_{i=1}^{d} V_i + \sum_{i<j}^{d} V_{ij} + ...+V_{1,2...,d},$$

with,

$$V_i = Var_{X_i}(E_{\mathbf{X}_{\sim i}}(Y|X_i)),$$

$$V_{ij} = Var_{X_{ij}}(E_{\mathbf{X}_{\sim ij}}(Y|X_i, X_j)) - V_i - V_j.$$

From this the Sobol indices can be computed as,

$$S_i = \frac{V_i}{Var(Y)}$$

and the total-effect index as,

$$S_{T,i} = 1 - \frac{Var_{\mathbf{X}_{\sim i}}(E_{X_i}(Y|\mathbf{X}_{\sim i}))}{Var(Y)}.$$

Appendix B

B.1. Overview of experiments and goodness-of-fit

The trained equation for the least squares multiple regression includes all first order interactions,

$$\frac{d\mathbf{R}(t)}{dt} = 230.02\,i - 86.64\,C_e - 129.75\,v + 14.81\,C_e\,v + 13.87\,C_e\,i - 45.10\,v\,i \tag{7}$$

Appendix C. Supplementary material

Supplementary data associated with this article can be found, in the online version, at https://doi.org/10.1016/j.seppur.2020.116939.

References

[1] M. Fitzpatrick, P. Champagne, M.F. Cunningham, R.A. Whitney, A biorefinery processing perspective: Treatment of lignocellulosic materials for the production of value-added products, Bioresour. Technol. 101 (23) (2010) 8915–8922, https://doi.org/10.1016/j.biortech.2010.06.125 ISSN 0960-8524.

[2] A. Campione, L. Gurreri, M. Ciofalo, G. Micale, A. Tamburini, A. Cipollina, Electrodialysis for water desalination: A critical assessment of recent developments on process fundamentals, models and applications, Desalination 434 (October 2017) (2018) 121–160, https://doi.org/10.1016/j.desal.2017.12.044, ISSN 00119164.

[3] G. Daufin, J.P. Escudier, H. Carrére, S. Bérot, L. Fillaudeau, M. Decloux, Recent and emerging applications of membrane processes in the food and dairy industry, Food Bioprod. Process.: Trans. Ins. Chem. Eng., Part C 79 (2) (2001) 89–102, https://doi.org/10.1016/S0960-3085(01)70244-1 ISSN 09603085.

[4] Z. Zhao, S. Shi, H. Cao, Y. Li, B. Van der Bruggen, Comparative studies on fouling of homogeneous anion exchange membranes by different structured organics in electrodialysis, J. Environ. Sci. (China) 77 (2019) 218–228, https://doi.org/10.1016/j.jes.2018.07.018 ISSN 18787320.

[5] X. Qian, M. Malmali, S.R. Wickramasinghe, Membranes for the removal of fermentation inhibitors from biofuel production, Elsevier Ltd, 2016, https://doi.org/10.1016/B978-0-08-100451-7.00009-8, ISBN 9780081004524.

[6] L.T.P. Trinh, C. Kundu, J.W. Lee, H.J. Lee, An integrated detoxification process with electrodialysis and adsorption from the hemicellulose hydrolysates of yellow poplars, Bioresour. Technol. 161 (March) (2014) 280–287, https://doi.org/10.1016/j.biortech.2014.03.042 ISSN 18732976.

[7] O. Kattan, Membranes in the biobased economy: electrodialysis of amino acids for the production of biochemicals, Ph.D. thesis University of Twente, 2013.

[8] A. Luiz, D.D. McClure, K. Lim, G. Leslie, H.G. Coster, G.W. Barton, J.M. Kavanagh, Potential upgrading of bio-refinery streams by electrodialysis, Desalination 415 (October 2016) (2017) 20–28, https://doi.org/10.1016/j.desal.2017.02.023 ISSN 00119164.

[9] L. Fu, X. Gao, Y. Yang, F. Aiyong, H. Hao, C. Gao, Preparation of succinic acid using bipolar membrane electrodialysis, Sep. Purif. Technol. 127 (2014) 212–218, https://doi.org/10.1016/j.seppur.2014.02.028 ISSN 13835866.

[10] M. Bdiri, L. Dammak, C. Larchet, F. Hellal, M. Porozhnyy, E. Nevakshenova, N. Pismenskaya, V. Nikonenko, Characterization and cleaning of anion-exchange membranes used in electrodialysis of polyphenol-containing food industry solutions; comparison with cation-exchange membranes, Separat. Purif. Technol. 210

(August 2018) (2019) 636–650, https://doi.org/10.1016/j.seppur.2018.08.044, ISSN 18733794.
[11] V.D. Grebenyuk, R.D. Chebotareva, S. Peters, V. Linkov, Surface modification of anion-exchange electrodialysis membranes to enhance anti-fouling characteristics, Desalination 115 (3) (1998) 313–329, https://doi.org/10.1016/S0011-9164(98)00051-4 ISSN 00119164.
[12] S. Mikhaylin, L. Bazinet, Fouling on ion-exchange membranes: Classification, characterization and strategies of prevention and control, Adv. Colloid Interf. Sci. (December) (2015), https://doi.org/10.1016/j.cis.2015.12.006.
[13] H. Guo, L. Xiao, S. Yu, H. Yang, J. Hu, G. Liu, Y. Tang, Analysis of anion exchange membrane fouling mechanism caused by anion polyacrylamide in electrodialysis, Desalination 346 (2014) 46–53, https://doi.org/10.1016/j.desal.2014.05.010 ISSN 00119164.
[14] P. Sosa-Fernandez, S. Miedema, H. Bruning, F. Leermakers, H. Rijnaarts, J. Post, Influence of solution composition on fouling of anion exchange membranes desalinating polymer-flooding produced water, J. Colloid Interface Sci. 557 (2019) 381–394, https://doi.org/10.1016/j.jcis.2019.09.029 ISSN 00219797.
[15] H.-J. Lee, S.-H. Moon, Influences of colloidal stability and electrokinetic property on electrodialysis performance in the presence of silica sol, J. Colloid Interface Sci. 270 (2) (2004) 406–412, https://doi.org/10.1016/j.jcis.2003.08.042 URL https://linkinghub.elsevier.com/retrieve/pii/S0021979703008592 . ISSN 00219797.
[16] H.-J. Lee, D.H. Kim, J. Cho, S.-H. Moon, Characterization of anion exchange membranes with natural organic matter (NOM) during electrodialysis, Desalination 151 (1) (2003) 43–52, https://doi.org/10.1016/S0011-9164(02)00971-2 URL http://linkinghub.elsevier.com/retrieve/pii/S0011916402009712 . ISSN 00119164.
[17] E. Korngold, F. de Körösy, R. Rahav, M. Taboch, Fouling of anionselective membranes in electrodialysis, Desalination 8 (2) (1970) 195–220, https://doi.org/10.1016/S0011-9164(00)80230-1 URL http://linkinghub.elsevier.com/retrieve/pii/S0011916400802301 . ISSN 00119164.
[18] E. Kobus, P. Heertjes, The poisoning of anion-selective membranes by humic substances, Desalination 12 (3) (1973) 333–342, https://doi.org/10.1016/S0011-9164(00)80098-3 URL https://linkinghub.elsevier.com/retrieve/pii/S0011916400800983 . ISSN 00119164.
[19] W. Wang, R. Fu, Z. Liu, H. Wang, Low-resistance anti-fouling ion exchange membranes fouled by organic foulants in electrodialysis, Desalination 417 (May) (2017) 1–8, https://doi.org/10.1016/j.desal.2017.05.013 ISSN 00119164.
[20] G. Grossman, A.A. Sonin, Membrane fouling in electrodialysis: a model and experiments, Desalination 12 (1) (1973) 107–125, https://doi.org/10.1016/S0011-9164(00)80178-2 ISSN 00119164.
[21] R. Audinos, Fouling of ion-selective membranes during electrodialysis of grape must, J. Membrane Sci. 41 (C) (1989) 115–126, https://doi.org/10.1016/S0376-7388(00)82395-9. ISSN 03767388.
[22] F.J. Rodríguez, L.A. Núñez, Characterization of aquatic humic substances, Water Environ. J. 25 (2) (2011) 163–170, https://doi.org/10.1111/j.1747-6593.2009.00205.x. ISSN 17476585.
[23] M.J. Corbatón-Báguena, M.C. Vincent-Vela, J.M. Gozálvez-Zafrilla, S. Álvarez-Blanco, J. Lora-García, D. Catalán-Martínez, Comparison between artificial neural networks and Hermia's models to assess ultrafiltration performance, Sep. Purif. Technol. 170 (2016) 434–444, https://doi.org/10.1016/j.seppur.2016.07.007 ISSN 18733794.
[24] C.M. Chew, M.K. Aroua, M.A. Hussain, Advanced process control for ultrafiltration membrane water treatment system, J. Clean. Prod. 179 (2018) 63–80, https://doi.org/10.1016/j.jclepro.2018.01.075 URL https://linkinghub.elsevier.com/retrieve/pii/S0959652618300830 . ISSN 09596526.
[25] E.A. Roehl, D.A. Ladner, R.C. Daamen, J.B. Cook, J. Safarik, D.W. Phipps, P. Xie, Modeling fouling in a large RO system with artificial neural networks, J. Membrane Sci. 552 (July 2017) (2018) 95–106, https://doi.org/10.1016/j.memsci.2018.01.064, https://linkinghub.elsevier.com/retrieve/pii/S0376738817318665. ISSN 03767388.
[26] F.E. Ahmed, R. Hashaikeh, A. Diabat, N. Hilal, Mathematical and optimization modelling in desalination: State-of-the-art and future direction, Desalination 469 (July) (2019) 114092, https://doi.org/10.1016/j.desal.2019.114092 URL https://linkinghub.elsevier.com/retrieve/pii/S0011916419312366 . ISSN 00119164.
[27] M. Bagheri, A. Akbari, S.A. Mirbagheri, Advanced control of membrane fouling in filtration systems using artificial intelligence and machine learning techniques: A critical review, Process Saf. Environ. Prot. 123 (2019) 229–252, https://doi.org/10.1016/j.psep.2019.01.013 URL https://linkinghub.elsevier.com/retrieve/pii/S0957582018310863 . ISSN 09575820.
[28] S. Park, S.-S. Baek, J. Pyo, Y. Pachepsky, J. Park, K.H. Cho, Deep neural networks for modeling fouling growth and flux decline during NF/RO membrane filtration, J. Membr. Sci. 587 (June) (2019) 117164, https://doi.org/10.1016/j.memsci.2019.06.004 URL https://linkinghub.elsevier.com/retrieve/pii/S0376738819301814 . ISSN 03767388.
[29] R. Goebel, M. Skiborowski, Machine-based learning of predictive models in organic solvent nanofiltration: Pure and mixed solvent flux, Sep. Purif. Technol. 237 (2020) 116363, https://doi.org/10.1016/j.seppur.2019.116363 ISSN 18733794.
[30] R.T.Q. Chen, Y. Rubanova, J. Bettencourt, D. Duvenaud, Neural Ordinary Differential Equations, CoRR abs/1806.0 (NeurIPS), http://arxiv.org/abs/1806.07366.
[31] Y. Lecun, Y. Bengio, G. Hinton, Deep learning, Nature 521 (7553) (2015) 436–444, https://doi.org/10.1038/nature14539 ISSN 14764687.
[32] R. Badrnezhad, B. Mirza, Modeling and optimization of cross-flow ultrafiltration using hybrid neural network-genetic algorithm approach, J. Ind. Eng. Chem. 20 (2) (2014) 528–543, https://doi.org/10.1016/j.jiec.2013.05.012 URL https://linkinghub.elsevier.com/retrieve/pii/S1226086X13002177 . ISSN 1226086X.
[33] S. Al Aani, T. Bonny, S.W. Hasan, N. Hilal, Can machine language and artificial intelligence revolutionize process automation for water treatment and desalination?, Desalination 458 (February) (2019) 84–96, https://doi.org/10.1016/j.desal.2019.02.005, https://linkinghub.elsevier.com/retrieve/pii/S0011916419300463. ISSN 00119164.
[34] Y. Lu, A. Zhong, Q. Li, B. Dong, Beyond finite layer neural networks: Bridging deep architectures and numerical differential equations, in: 35th International Conference on Machine Learning, ICML 2018 7, 2018, pp. 5181–5190.
[35] W. Yuan, A. Kocic, A.L. Zydney, Analysis of humic acid fouling during microfiltration using a pore blockage–cake filtration model, J. Membr. Sci. 198 (1) (2002) 51–62, https://doi.org/10.1016/S0376-7388(01)00622-6 URL https://linkinghub.elsevier.com/retrieve/pii/S0376738801006226 . ISSN 03767388.
[36] C.Y. Tang, Q. She, W.C. Lay, R. Wang, A.G. Fane, Coupled effects of internal concentration polarization and fouling on flux behavior of forward osmosis membranes during humic acid filtration, J. Membr. Sci. 354 (1–2) (2010) 123–133, https://doi.org/10.1016/j.memsci.2010.02.059 URL https://linkinghub.elsevier.com/retrieve/pii/S037673881000181X . ISSN 03767388.
[37] J. Shao, J. Hou, H. Song, Comparison of humic acid rejection and flux decline during filtration with negatively charged and uncharged ultrafiltration membranes, Water Res. 45 (2) (2011) 473–482, https://doi.org/10.1016/j.watres.2010.09.006 URL https://linkinghub.elsevier.com/retrieve/pii/S0043135410006354 . ISSN 00431354.
[38] P. Atkins, J. de Paula, Physical Chemistry: Thermodynamics, Structure, and Change, tenth ed., Freeman, W.H., 2014, ISBN 9780716787594.
[39] Y. Tanaka, Ion Exchange Membranes Fundamentals and Applications, second ed., Elsevier, Amsterdam, Netherlands, 2015, ISBN 9780444519825.
[40] P. Bogacki, L. Shampine, A 3(2) pair of Runge - Kutta formulas, Appl. Mathe. Lett. 2 (4) (1989) 321–325, https://doi.org/10.1016/0893-9659(89)90079-7 URL https://linkinghub.elsevier.com/retrieve/pii/0893965989900797 . ISSN 08939659.
[41] J. Bezanson, A. Edelman, S. Karpinski, V.B. Shah, Julia: A fresh approach to numerical computing, SIAM Rev. 59 (1) (2017) 65–98, https://doi.org/10.1137/141000671 URL https://epubs.siam.org/doi/10.1137/141000671 . ISSN 00361445.
[42] C. Rackauckas, M. Innes, Y. Ma, J. Bettencourt, L. White, V. Dixit, DiffEqFlux.jl - A Julia Library for Neural Differential Equations (2019) 1–17, URL http://arxiv.org/abs/1902.02376.
[43] D.P. Kingma, J. Ba, Adam: A Method for Stochastic Optimization (2014) 1–15, URL http://arxiv.org/abs/1412.6980.
[44] A. Saltelli, M. Ratto, T. Andres, F. Campolongo, J. Cariboni, D. Gatelli, M. Saisana, S. Tarantola, Global Sensitivity Analysis. The Primer, John Wiley & Sons Ltd, Chichester, UK, 2007, https://doi.org/10.1002/9780470725184 ISBN 9780470725184.
[45] I. Sobol, Sensitivity estimates for nonlinear mathematical models, Mathe. Modell. Civil Eng. 1 (4) (1993) 407–414, ISSN 18129471.
[46] Bram De Jaegher, Eneko Larumbe, Wim De Schepper, Arne Verliefde, Ingmar Nopens, Data on ion-exchange membrane fouling by humic acid during electrodialysis, Data in Brief, 2020, https://doi.org/10.1016/j.seppur.2020.116939.
[47] R.W. Field, D. Wu, J.A. Howell, B.B. Gupta, Critical flux concept for microfiltration fouling, J. Membr. Sci. 100 (3) (1995) 259–272, https://doi.org/10.1016/0376-7388(94)00265-Z ISSN 03767388.
[48] V.V. Nikonenko, N.D. Pismenskaya, E.I. Belova, P. Sistat, P. Huguet, G. Pourcelly, C. Larchet, Electrodialysis for water desalination: A critical assessment of recent developments on process fundamentals, models and applications, Adv. Colloid Interface Sci. 160 (1–2) (2010) 101–123, https://doi.org/10.1016/j.cis.2010.08.001 ISSN 00018686.
[49] G. James, T. Hastie, R. Tibshirani, D. Witten, An Introduction to Statistical Learning: With Applications in R, Springer US, New York, 2013.